IEEE Access
Multidisciplinary | Rapid Review | Open Access Journal

Received 27 October 2023, accepted 19 November 2023, date of publication 24 November 2023,
date of current version 5 December 2023.

Digital Object Identifier 10.1109/ACCESS.2023.3336769

RESEARCH ARTICLE

Research on Reliability Growth of Shock Absorption System in Rapid Secure Device of Shipboard Helicopter

ZHUXIN ZHANG[1,2], WEIJIAN LI[1,3], HUILIANG SUN[1,2], BING WANG[1,2], DINGXUAN ZHAO[1,3], AND TAO NI[1,2]

[1]Hebei Key Laboratory of Special Delivery Equipment, Yanshan University, Qinhuangdao 066004, China
[2]School of Vehicle and Energy, Yanshan University, Qinhuangdao 066004, China
[3]School of Mechanical Engineering, Yanshan University, Qinhuangdao 066004, China

Corresponding author: Weijian Li (lwj-mh@qq.com)

This work was supported in part by the Key Research and Development Program of Hebei Province under Grant 20353501D, Grant 21351802D, and Grant 22357601D; and in part by the Natural Science Foundation of Hebei Province under Grant E2020203174.

ABSTRACT Aiming the problem that the mechanical claw in very few rapid secure devices (RSD) failed to capture the fixed rod of the shipboard helicopter due to the lose effectiveness of the internal shock absorption system of the RSD, a reliability growth test bench is built to conduct a reliability growth test study on the shock absorption system in a single RSD test prototype. The fault locations are identified according to the fault phenomenon. After the fault causes are found, the reliability optimization designs of the shock absorption system are carried out and the optimization design schemes are determined. With the discrete army materiel systems analysis activity (AMSAA) model analysis method, according to the reliability growth test data of the test prototype, the maximum likelihood estimation of the model parameters is determined based on a genetic algorithm. A trend test for the reliability growth of the test prototype and goodness-of-fit test for the AMSAA model are performed, and the reliability estimation and lower confidence limit of the reliability of the test prototype in the final development stage of the shock absorption system are obtained. The test data and statistical inference indicate that the reliability optimization designs using scheme 2 in the first test stage and scheme 1 + scheme 2 in the second test stage are correct and feasible, which meets the reliability requirements that the RSD reliability is not less than 99.5% and improves the robustness of the shock absorption system. This study further provides data support for the reliability research of RSD, which is of great significance for improving the service capacity of RSD equipment and ensuring the life safety of shipboard helicopters.

INDEX TERMS Discrete AMSAA model, genetic algorithm, rapid secure device, reliability growth, shock absorption system.

NOMENCLATURE

$x1$	Moving distance when the buffer plate is squeezed.
$x2$	Distance between the buffer plate and the upper cover plate in the X-direction.
$N(t)$	Cumulative failure times of the product.
$E[N(t)]$	Mathematical expectation of the cumulative failure times.
t	Cumulative test time.
a	Scale parameter.
m	Growth rate.
b	Shape parameter.
$N(i)$	Cumulative number of failures of the product.
$E[N(i)]$	Mathematical expectation of the cumulative number of failures.
i	Cumulative test number.
c	Number of the test stages of the product.

The associate editor coordinating the review of this manuscript and approving it for publication was Rosario Pecora.

s_k	Number of the test failures in stage k.
i_k	Cumulative number of tests at the end of stage k.
R_k	Reliability of the product tested in stage k.
n_k	Number of tests in stage k.
p	Probability that event A will occur in each test.
$X = r$	The event A, which occurs exactly r times in h Bernoulli tests.
$\hat{a}$	Maximum likelihood estimation of a.
$\hat{b}$	Maximum likelihood estimation of b.
μ	Reliability growth trend test statistic.
μ_0	Critical value of μ.
M	Goodness-of-fit test parameter.
j	Cumulative number of failures of the product, $j = N(i)$.
$i_j{}'$	Cumulative number of tests up to j failures.
J	Cumulative number of tests at the end of the testing.
α	significance level.
$C^2(M)$	Goodness-of-fit test statistic.
$C^2(M, \alpha)$	Critical value of $C^2(M)$.
$\hat{R}_k$	Reliability estimate in stage k.
$\hat{s}_k$	Estimated number of the test failures in stage k.
$R_{k,L}$	Reliability lower confidence limit in stage k.
$z_{1-\alpha}$	1-α quantile of the standard normal distribution.
K_k	Cumulative number of failures up to stage k.
γ	Confidence level.
$\hat{R}_{k,L}$	Maximum likelihood estimate of the reliability lower confidence limit in stage k.

I. INTRODUCTION

Shipboard helicopters use ship decks as take-off and landing platforms and can perform anti-submarine, early warning, reconnaissance, transportation, aerial survey, and search-and-rescue operations and other tasks [1], [2]. When shipboard helicopters are carried on board medium and small ships, owing to the small deck platform, complex environment of the ship's roll motion, pitch motion, heave motion, high-speed navigation, unstable air flow field, and so on [3], [4], landing on the ship deck will be difficult for the shipboard helicopters, which can seriously affect the sea and air integration development process of each country. Therefore, to improve the rate of attendance and safety of shipboard helicopters under severe sea conditions, developing a special assisted landing and towing system for shipboard helicopters has become a consensus. The main types of assisted landing and towing systems include the Russian assisted landing net and winch towing system [5]; harpoon-grille-type assisted landing device and SAMACH towing system developed by DCNS, France [6], [7]; and US Curtiss-Wright's shipboard helicopter landing assistance and fixation (E) system [8], recovery assist secure and traverse (RAST) system [9], aircraft ship integrated secure and traverse (ASIST) system [10], [11], and twin claw-ASIST system [12]. Currently, China has two main types of shipboard helicopters, namely, the Ka-28 and the Z-9 [13], [14]. The Ka-28 adopts the Russian assisted landing net and winch towing system, in which the assisted landing net is mainly used to increase the friction between the tires and the deck when the shipboard helicopter lands on the ship deck to prevent it from skidding. However, the assisted landing net has no mooring function. Under the condition of ship deck rolling and pitching, the assisted landing net will not prevent the shipboard helicopter from overturning. Moreover, laying the assisted landing net before the shipboard helicopter takes off and lands is time consuming, involving many operators and a low degree of automation [15]. The Zhi-9 adopts the French harpoon-grille-type assisted landing device and SAMACH towing system, in which the assisted landing device can complete the rapid mooring operation only under certain sea conditions, such as ship roll of no more than $\pm 7.5°$, pitch of $\pm 2°$, and wind speed of 20 m/s, and is applicable only to small shipboard helicopters, with a self-weight of less than 5 t [16], [17]. Therefore, shipboard helicopter assisted landing and towing systems have become a short board, restricting the development of the combat effectiveness of Chinese shipboard helicopters. To break the technical blockade of foreign countries in the field of shipboard helicopter assisted landing, China started independently developing the most advanced third-generation shipboard helicopter assisted landing and towing system in the world, which is an ASIST system. The ASIST system is composed of two sets of devices installed on the helicopter and ship. The shipboard device mainly includes a hydraulic power system (hydraulic winch), a rapid secure device (RSD) [18], a preset track, an infrared tracker, a pilot visual indicator, and so on. The airborne device mainly includes a helicopter abdominal fixed rod and laser target source [19]. The design idea of the system is mainly to assist a shipboard helicopter in landing on the deck of a ship, and rapid capturing of the helicopter abdominal fixed rod, rapid mooring, straightening, towing into the hangar, towing out of the hangar, unlocking, and releasing. The ASIST system has the characteristics of a high degree of automation, short-time and high-accuracy shipboard helicopter deck landing, and undoubtedly represents the development direction of the most advanced technology in the field.

As an integral component of the ASIST system, the RSD performs important tasks such as capturing, mooring, straightening, and transferring the shipboard helicopter to designated locations. The high reliability of RSD operations is an important guarantee for the reliable operation of the ASIST system. Therefore, examining the reliability growth of the RSD is essential. In the field of reliability, reliability growth models mainly include the discrete growth model, which is applicable to success/failure products or non-repairable life products, and the continuous growth model, which is applicable to repairable products for continuous

work [20], [21]. Currently, the two growth models with milestone significance are the Duane model (continuous) and army materiel systems analysis activity (AMSAA) model (continuous/discrete) [22], [23], [24], [25]. With the proposed of these two reliability growth models, domestic reliability engineering researchers conducted abundant research on the reliability growth of hydraulic systems, electronic products, and aerospace products [26], [27], [28], [29], [30]. However, research on the reliability growth of nautical-class shipboard helicopter assisted landing systems and other aspects is lacking.

The first RSD in China was successfully developed by Dingxuan Zhao's team at Yanshan University and has been successfully delivered to the Chinese navy. However, during the joint commissioning, mooring, and navigation testing for each RSD, it was observed that the mechanical claw in very few RSDs failed to capture the shipboard helicopter fixed rod due to the failure of their internal shock absorption system. To realize the reliability growth of an RSD, in this study, by designing and developing a dedicated reliability growth test bench and formulating test mission profiles, fault excitation, fault analysis, and reliability optimization design are conducted in a planned manner for the shock absorption system in a single RSD test prototype to solve the design defects. a discrete AMSAA model is used to make statistical inference on the reliability of the test prototype shock absorption system based on the test data, in order to prove with expectation the correctness and feasibility of the reliability optimization design, and further provide data support for the study of the reliability growth of the RSD whole equipment.

II. RELIABILITY OPTIMIZATION DESIGN OF RSD SHOCK ABSORPTION SYSTEM

A. STRUCTURE AND WORKING PRINCIPLE OF RSD SHOCK ABSORPTION SYSTEM

The two-dimensional structure diagram of RSD is shown in Figure 1, where the number 11 represents the shock absorption system in RSD. The system is composed of a detection limit switch 1, when the buffer plate is compressed in place (hereinafter referred to as limit switch 1); a shock absorbing and cushioning spring; limit copper blocks 1 and 2; a buffer plate; and so on.

The system's working principle is as follows: when the shipboard helicopter lands on the ship deck, the hydraulic winch will pull the RSD to quickly approach the helicopter belly fixed rod in the positive X-direction. After the buffer plate collides with the fixed rod, the fixed rod pushes the buffer plate in the negative X-direction, and the shock absorbing and cushioning spring is compressed. When the buffer plate is squeezed in place, that is, the extrusion displacement is $x1$, limit switch 1 will be triggered, and the control system will send a mechanical claw capture command. The mechanical claw quickly captures the fixed rod in the positive Y-direction, and the RSD completes the rapid capture helicopter operation. When the RSD release helicopter is operated, the mechanical claw is first retracted along the negative Y-direction. At this time, the RSD retracts along the negative X-direction, and the buffer plate is reset under the action of the shock absorbing and cushioning spring. Figure 2 presents a physical diagram of the RSD.

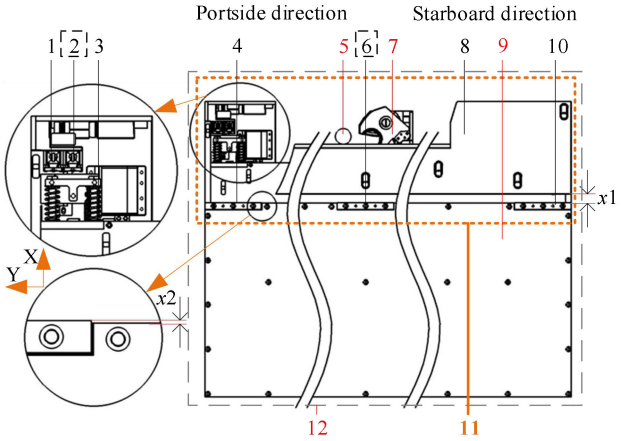

FIGURE 1. Two-dimensional structure diagram of RSD: 1. Limit switch 1, 2. Limit switch 2, 3. Shock absorbing and cushioning spring, 4. Limit copper block 1, 5. Fixed rod, 6. Limit copper block 3, 7. Mechanical claw, 8. Buffer plate, 9. Upper cover plate, 10. Limit copper block 2, 11. Shock absorption system, and 12. RSD.

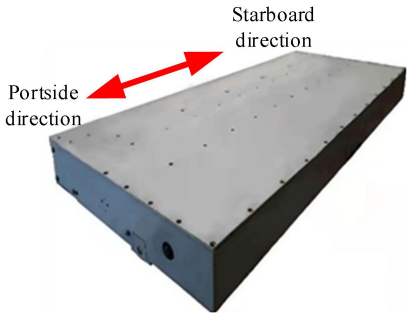

FIGURE 2. Physical diagram of RSD.

B. RELIABILITY TEST AND FAULT PHENOMENON OF TEST PROTOTYPE

Figure 3 presents the RSD reliability growth test bench. The test prototype is fixedly connected to the track slider of the test bench. The two ends of the bottom of the track slider are flexibly connected to the two ends of an X-direction parallel-connection double-extension piston rod hydraulic cylinder with a steel cable.The tension force of the steel cable is 20 kN. When the quick capture command is executed on the test prototype, under the action of the parallel-connection double-extension piston rod hydraulic cylinder, the test prototype will quickly approach and collide with the helicopter's simulated fixed rod along the deck simulation track in the positive X-direction at a speed of up to 1.5 m/s peak to trigger the Y-direction fast-capture function of the mechanical claw and complete the capture operation for the simulated fixed rod. The simulated fixed rod can be anywhere in the 2.0 m capture area of the mechanical claw of the test prototype along the Y-direction.

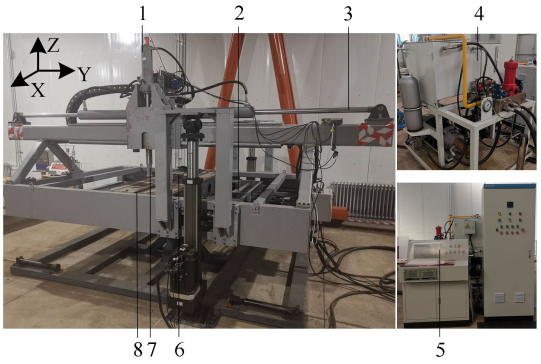

FIGURE 3. Physical diagram of RSD reliability growth test bench: 1. Z-direction single-extension piston rod hydraulic cylinder, 2. X-direction parallel-connection double-extension piston rod hydraulic cylinder, 3. Y-direction double-extension piston rod hydraulic cylinder, 4. Hydraulic pump station, 5. Console, 6. Track slider, 7. Simulated fixed rod, and 8. Deck simulation track.

In an environment with a temperature of about 25 °C and humidity of about 40%, the reliability growth test bench is used to conduct the test task cycle, according to the mission profile in Figure 4.

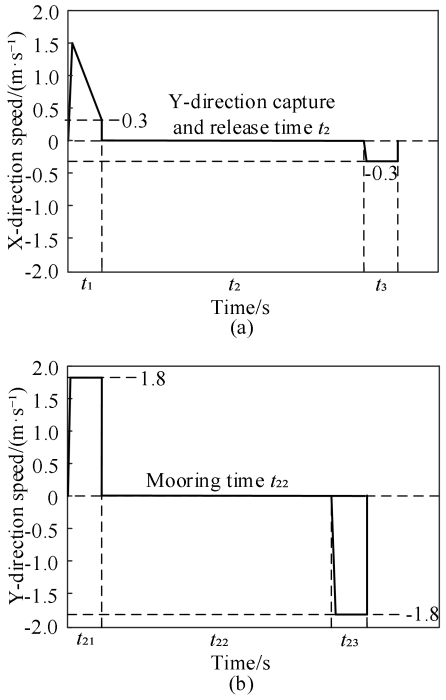

FIGURE 4. Mission profile of RSD in a test cycle: (a) Mission profile of the RSD approaching/away from the simulated fixed rod in the X-direction; (b) Mission profile of the RSD mechanical claw capture/ release the simulated fixed rod in the Y-direction.

The process is as follows: In the t_1 time period, the test prototype rapidly approaches and collides with the simulated fixed rod in the positive X-direction at the initial position. When the buffer plate is squeezed in place, the Y-direction capture function of the mechanical claw will be triggered. In the t_{21} time period, the mechanical claw performs the Y-direction capture function. In the t_{22} time period, the mechanical claw performs the mooring function. In the t_{23} time period, the mechanical claw performs the Y-direction release function. In the t_3 time period, the test prototype is far from the simulated fixed rod in the X-direction and returns to the initial position. Based on the condition that the mean cycles between failures of the RSD capture/release specified in the R&D assignment is not less than 200, the test prototype in this study has carried out 218 reliability cycle tests, and a total of 5 failure phenomena of mechanical claw capture the simulated fixed rod of the test prototype occurred.

C. FAULT CAUSE ANALYSIS OF TEST PROTOTYPE

After the buffer plate is squeezed in place, while observing the RSD console interface, it is found that limit switch 1 does not send an immediate signal. After being stationary for a period of time, the equipment suddenly sends a signal automatically. After limit switch 1 is replaced with a new switch, the equipment fault is eliminated. According to the above description, it is believed that the failure of the mechanical claw to capture the simulated fixed rod of the test prototype is caused by the limit switch 1 damage.

As shown in Figure 5, the white line is the normally closed contacts voltage of the faulty limit switch 1, which decreases over time. Through the repeat compression of limit switch 1 and measurement of its resistance value with a multimeter, it is determined that the resistance value, measured each time, has a large difference, and the resistance value changes automatically and continuously under a static measurement. Among the limit switches that failed in the RSD joint commissioning, mooring, navigation and reliability cycle test, two limit switches are randomly sampled as failure samples to analyze the cause of the failure.

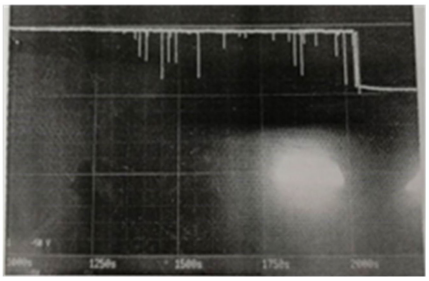

FIGURE 5. Contact voltage change curve of limit switch.

The outer cover metal plates of the two limit switch failure samples are opened, and X-ray state detection is conducted for the two limit switch failure samples under the free and pressed state of the push rod. The internal structure (components 1 to 14) of the two limit switch failure samples is not found to be abnormal, as shown in Figure 6.

The two limit switch failure samples are pressed 10 times repeatedly, and the waveforms in the process of contacts closing and breaking during each action are tested. The results show that when the normally closed contacts are in the power-off state, the normally open contacts will remain in the power-off state, the failure phenomenon of sample 1 is more serious, and the normally open contacts of sample 2 have a virtual connection state, as shown in Figure 7.

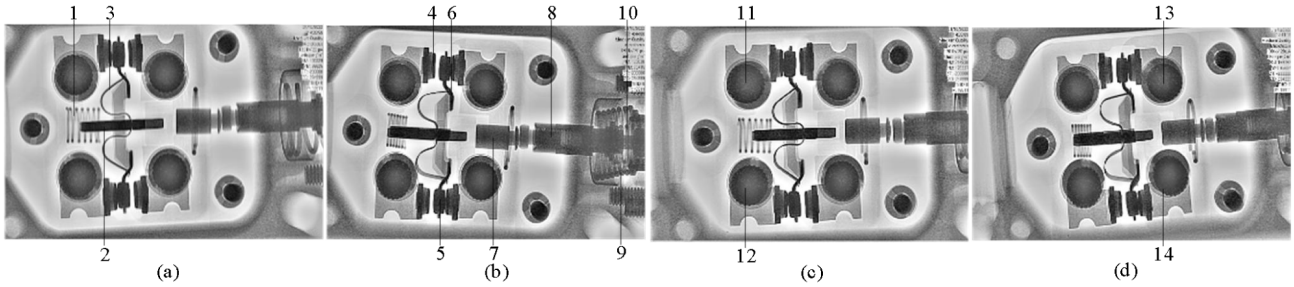

FIGURE 6. X-ray status detection diagram of limit switches: (a) Sample 1 in free state. 1. Contact seat push rod spring, 2. Contact seat push rod, 3. Contact seat curved sheet spring; (b) Sample 1 in compressed state. 4. Static contact, 5. Moving contact, 6. Moving contact spring support, 7. Slider, 8. Push rod, 9. Push rod large spring, 10. Push rod small spring; (c) Sample 2 in free state. 11. Normally closed contact connection point 1, 12. Normally closed contact connection point 2; (d) Sample 2 in compressed state. 13. Normally open contact connection point 1, 14. Normally open contact connection point 2.

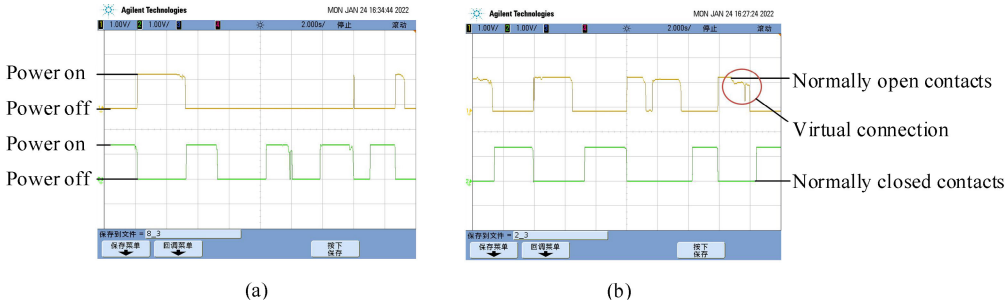

FIGURE 7. Limit switch waveform test diagram: (a) Sample 1; (b) Sample 2.

The normally open/closed contact connection points of the two limit switch failure samples are connected by guide wires to test the contact state of the normally open/closed contacts. The results show that the normally open contacts of sample 1 are not energized, the normally closed contacts are 246 mΩ, the normally open contacts of sample 2 are 396 mΩ, and the normally closed contacts are 12.7 mΩ. Only the contact resistance value of the normally closed contacts of sample 2 is less than the max. 15 mΩ in the technical index, whereas the other are out of tolerance in different degrees.

The morphology of the contact parts of the two limit switch failure samples is examined, and an organic contamination film is found on the surface of the normally open contact of failure sample 1 as well as white organic residue particles on the surface of the remaining contacts, as shown in Figure 8.

On the basis of the above analysis, it can be concluded that the reason for the failure of the mechanical claw of the test prototype to capture the simulated fixed rod is the presence of an organic contamination film or organic residue particles on the contact surfaces of the limit switches formed under the action of the electric field, which can cause the resistance of the closed contacts to become larger/unstable, or the contacts are impassable, and then the failure phenomenon of power off or virtual connection of the limit switches occurs.

D. RELIABILITY OPTIMIZATION DESIGN OF SHOCK ABSORPTION SYSTEM OF TEST PROTOTYPE

Two reliability optimization design schemes are selected in this study. Scheme 1 is to use heavy current to arc clean the contact surfaces of the limit switches. The power on/power off states of sample 1 and sample 2 are tested (with a voltage of 10 V) at 0.2 A, 1 A, and 2 A currents. The results show that as the test current increases, the fault phenomenon gradually decreases in sample 1 and sample 2. In the 2 A current test, the fault phenomenon does not recur. The test results are shown in Figure 9.

However, the heavy-current arc-cleaning contacts scheme is not adopted in this study, because evaluating the cleaning time node is difficult as well as monitoring the health status of the limit switch in real time after cleaning, which cannot ensure that the fault phenomenon will not recur. Scheme 2 adopts the redundancy design method of the limit switches, as shown in Figure 1. Limit switch 1 and limit switch 2 are used in parallel. When the buffer plate is compressed in place by the simulated fixed rod, the two limit switch rollers will be compressed, and the control program will self-check. When any limit switch is triggered, the mechanical claw can execute the fast capture command, and the RSD console can detect the power-on and power-off status of the two limit switches in real time. The robustness of the shock absorption system is improved. Therefore, in this study, scheme 2 is adopted for the reliability optimization design of the shock absorption system of the test prototype.

III. RELIABILITY GROWTH TEST OF SHOCK ABSORPTION SYSTEM OF TEST PROTOTYPE

A. PROCESS AND EFFECT OF RELIABILITY GROWTH TEST

After the reliability optimization design of the shock absorption system of the test prototype is conducted with scheme 2,

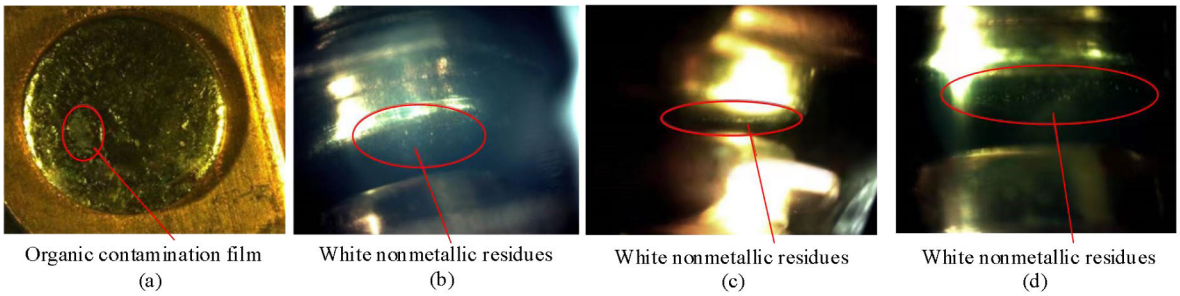

FIGURE 8. Limit switches contact surface detection diagram: (a) Normally open contact in sample 1; (b) Normally close contact in sample 1; (c) Normally open contact in sample 2; (d) Normally close contact in sample 2.

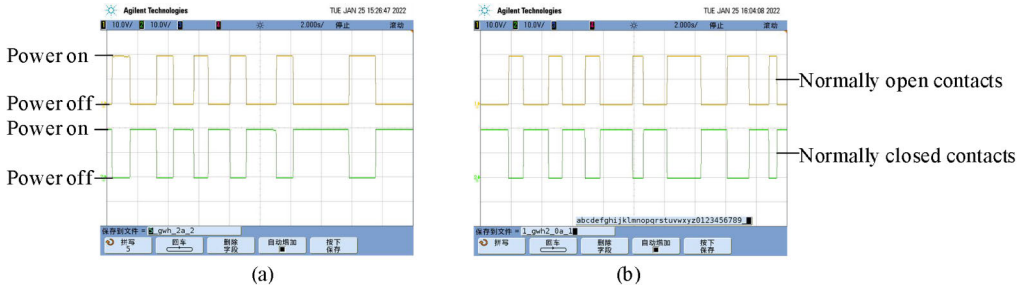

FIGURE 9. Limit switches waveform test diagram under 2 A current: (a) Sample 1; (b) Sample 2.

according to the same operation conditions as those in the reliability test stage, the delayed correction strategy is adopted. In the second test phase, two failures of the mechanical claw of the test prototype to capture the simulated fixed rod are recorded. All the tests in the third phase are successful. The cumulative number of tests, number of test failures, and number of tests in each stage are shown in Table 1.

A total of 7 class B failures (two failure modes) are observed during the prototype testing (class B failures are systematic failures that need to be corrected). After the stage test, the shock absorption system of the test prototype is optimally designed, and the reliability growth test is continued in the next phase.

TABLE 1. Cumulative failure data of total test time of test prototype.

Test phase k	Cumulative number of tests i_j'	Number of test failures $N(i)$	Number of tests n_k
1	5	1	
1	28	2	
1	59	3	218
1	131	4	
1	218	5	
2	373	6	207
2	425	7	
3	655	7	230

B. FAULT ANALYSIS AND OPTIMIZATION DESIGN OF TEST PROTOTYPE IN THE SECOND STAGE

1) FAULT CAUSE ANALYSIS OF TEST PROTOTYPE

When the mechanical claw of the test prototype fails to capture the simulated fixed rod twice, the failure phenomenon is observed each time that the mechanical claw cannot be closed smoothly. The mechanical claw can achieve the closing and opening functions, excluding the failure of the square shaft and connecting rod, by manually turning the square shaft and upper claw of the mechanical claw (the square shaft is rotated counterclockwise, and by driving the connecting rod, the upper claw of the mechanical claw can be opened). However, it is observed that at the test site, position 1, where the helicopter simulation fixed rod collides with the RSD buffer plate, is considerably worn down. The distance between the buffer plate wall surface and side wall surface of the lower claw of the mechanical claw is 2 mm in the X-direction; thus, when the impact position 1 of the simulated fixed rod is worn down more than 2 mm in the X-direction, the side wall surface of the lower claw of the mechanical claw will generate friction resistance in position 2, resulting in the fixed rod not being able to enter the mechanical claw smoothly and capture failure, as shown in Figure 10.

In addition, when the buffer plate is squeezed in place by the simulated fixed rod, both sides of the buffer plate will be subject to the support reaction of limit copper block 1 and limit copper block 2. However, the other parts of the buffer plate have no force support in the X-direction, resulting in elastic deformation of the buffer plate under the action of the simulated fixed rod extrusion load (in the case of no elastic deformation, the distance between the buffer plate and the upper cover plate in the X-direction is $x2$), $x2$ will decrease, as shown in Figure 1. Under this condition, the distance between the buffer plate wall surface and side wall surface of the lower claw of the mechanical claw will be less than 2 mm in the X-direction. when the impact position 1 of

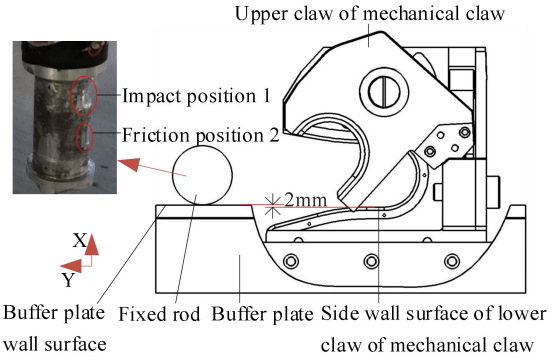

FIGURE 10. Structure diagram of mechanical claw capture/release of simulated fixed rod.

the simulated fixed rod is worn down less than 2 mm in the X-direction, the side wall surface of the lower claw of the mechanical claw will also due to the friction resistance in position 2, resulting in the simulated fixed rod not being able to enter the mechanical claw smoothly and capture failure.

For the process of the RSD fast approaching, colliding with, and extruding the simulated fixed rod in the X-direction, the simulated fixed rod load measurement test is performed. The distance between the position of the simulated fixed rod extruding the buffer plate and initial position of the mechanical claw is 869 mm (the squeezed position is close to the middle position of the buffer plate). The test curve is shown in Figure 11, where the peak 1 value is the instantaneous impact load of the RSD buffer plate colliding with the simulated fixed rod, and the peak 2 value is the instantaneous extrusion load of the RSD buffer plate being squeezed into place by the simulated fixed rod. After the buffer plate is squeezed in place, the force of the simulated fixed rod on the buffer plate is about 9000 N.

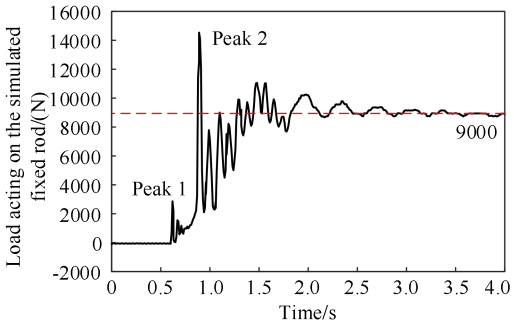

FIGURE 11. Load measurement test of simulated fixed rod.

As shown in Figure 12, the deformation value of the maximum displacement in the displacement nephogram is 0.635 mm, which is located at the site of contact with the simulated fixed rod, when an extrusion force of 9000 N is applied in the negative X-direction to the middle of the buffer plate. Therefore, under this working condition, when the wear of the impact position 1 of the simulated fixed rod is greater than 1.365 mm in the X-direction, the failure phenomenon of the mechanical claw not closing smoothly will occur.

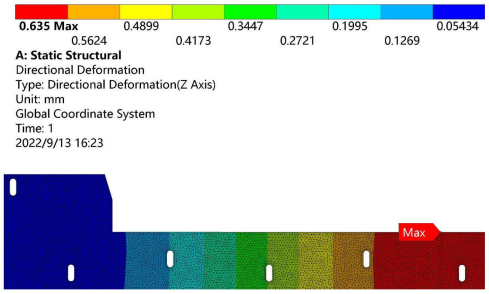

FIGURE 12. X-direction displacement nephogram before optimized design of buffer plate.

2) OPTIMIZATION DESIGN OF TEST PROTOTYPE

Meanwhile, two reliability optimization design schemes are adopted in this study. Scheme 1 involves adding limit copper block 3 in the middle of the RSD upper cover plate, as shown in Figure 1. The deformation value of the maximum displacement in the buffer plate displacement nephogram is 0.108 mm and 0.116 mm when an extrusion force of 9000 N is loaded in the negative X-direction at the positions shown in Figure 13. Scheme 2 involves replacing the simulated fixed rod or rotating the simulated fixed rod 90° to ensure that the wear of the impact position 1 of the simulated fixed rod in the X-direction is 0.

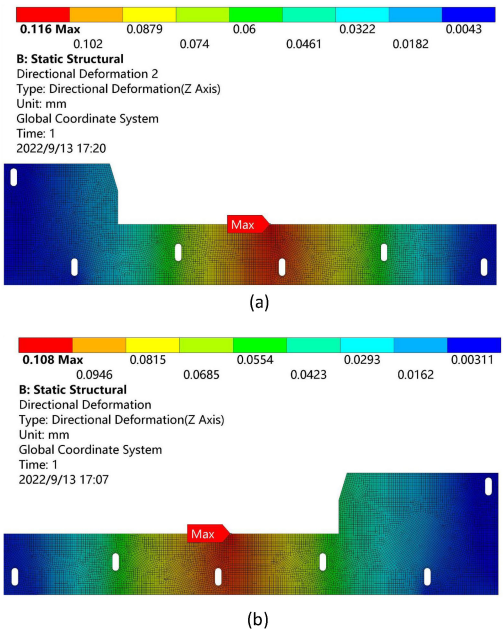

FIGURE 13. X-direction displacement nephogram after optimized design of buffer plate: (a) Middle position of limit copper block 1 and limit copper block 3; (b) Middle position of limit copper block 2 and limit copper block 3.

The simultaneous selection of the two schemes can not only reduce the maximum deformation value of the buffer

plate at the site of contact with the simulated probe rod, but also further increase the wear allowance of the simulated probe rod in the X-direction, which meets the design requirements of the simulated fixed rod captured by the mechanical claw and improves the robustness of the shock absorption system.

IV. RELIABILITY GROWTH MODEL OF SHOCK ABSORPTION SYSTEM OF RSD TEST PROTOTYPE

A. DISCRETE AMSAA MODEL WITH DELAYED CORRECTION STRATEGY

According to the mathematical description of the Duane model [31], the relationship between the mathematical expectation $E[N(t)]$ of the cumulative failure times of the product in the development period $(0, t]$ and cumulative test time t of the repairable product is obtained, that is, the characteristic of the continuous learning curve is

$$E\left[N\left(t\right)\right] = at^{1-m} = at^{b}, \tag{1}$$

where $N(t)$ is the cumulative failure times of the product, a is the scale parameter, m is the growth rate, and b is the shape parameter. According to Equation (1), the relationship between the mathematical expectation $E[N(i)]$ of the cumulative failure number of the product and cumulative test number i is obtained, the characteristic of the discrete learning curve is

$$E\left[N\left(i\right)\right] = ai^{1-m} = ai^{b}, \tag{2}$$

where $N(i)$ is the cumulative number of failures of the product. If the number of the test stages of the product is c, then the number of the test failures in stage k is

$$s_k = a\left(i_k^b - i_{k-1}^b\right), \tag{3}$$

where i_k is the cumulative number of tests at the end of phase k, and $1 \le k \le c$. It can be seen from Equation (3) that the reliability of the product tested in phase k is as follows:

$$R_k = 1 - s_k/n_k, \tag{4}$$

where n_k is the number of tests in phase k, and $n_k = i_k - i_{k-1}$. Equation (4) is the discrete AMSAA reliability growth model proposed by Crow. It can be seen from the derivation process that the number of tests in each stage of the product is known. After the completion of n_k tests, the optimal design of the product is realized, that is, the delayed correction strategy is adopted. The number of failures in each stage is random.

B. MAXIMUM LIKELIHOOD ESTIMATION OF MODEL PARAMETERS

It can be seen from the previous section that the number of failures in the n_k tests of stage k is s_k, and the tests in each stage follow a binomial distribution. Then, the probability function is

$$P\left(X = r\right) = C_h^r p^r \left(1-p\right)^{h-r}, \tag{5}$$

where $X = r$ is event A, which occurs exactly r times in h Bernoulli tests, and p is the probability that event A will occur in each test. According to Equation (5), the following likelihood function equation for a and b is constructed:

$$L\left(a, b\right) = \prod_{k=1}^{c} C_{n_k}^{s_k} \left(1 - R_k\right)^{s_k} R_k^{n_k - s_k}. \tag{6}$$

Merging Equation (4) and Equation (6), and logarithms are taken from both sides of the equation to obtain the logarithmic likelihood function equation, as follows:

$$\begin{aligned}\ln L\left(a, b\right) = &\sum_{k=1}^{c} \ln C_{n_k}^{s_k} + \sum_{k=1}^{c} s_k \ln \frac{a\left(i_k^b - i_{k-1}^b\right)}{n_k} \\ &+ \sum_{k=1}^{c} \left(n_k - s_k\right) \ln\left[1 - \frac{a\left(i_k^b - i_{k-1}^b\right)}{n_k}\right].\end{aligned} \tag{7}$$

The partial derivatives of $\ln L(a, b)$ for parameters a and b can be obtained, as follows:

$$\begin{cases} f_1\left(a, b\right) = \dfrac{\partial \ln L\left(a, b\right)}{\partial a} \\ = \displaystyle\sum_{k=1}^{c}\left[\frac{s_k}{a} - \frac{\left(n_k - s_k\right)\left(i_k^b - i_{k-1}^b\right)}{n_k - a\left(i_k^b - i_{k-1}^b\right)}\right] \\ f_2\left(a, b\right) = \dfrac{\partial \ln L\left(a, b\right)}{\partial b} \\ = \displaystyle\sum_{k=1}^{c}\left[\frac{s_k a\left(i_k^b \ln i_k - i_{k-1}^b \ln i_{k-1}\right)}{a\left(i_k^b - i_{k-1}^b\right)}\right. \\ \left. - \dfrac{\left(n_k - s_k\right) a\left(i_k^b \ln i_k - i_{k-1}^b \ln i_{k-1}\right)}{n_k - a\left(i_k^b - i_{k-1}^b\right)}\right]. \end{cases} \tag{8}$$

Let nonlinear Equation (8) be

$$\begin{cases} f_1\left(a, b\right) = 0 \\ f_2\left(a, b\right) = 0. \end{cases} \tag{9}$$

Then, the solutions of Equation (9) are the maximum likelihood estimation of a and b, that is, $\hat{a}$ and $\hat{b}$. The following equation is constructed according to Equation (9):

$$f\left(a, b\right) = f_1^2\left(a, b\right) + f_2^2\left(a, b\right). \tag{10}$$

That is, the problem of solving nonlinear Equation (9) is transformed into the following optimization problems:

$$\min f\left(a, b\right), a \in \left(0, 1\right), b \in \left(0, 1\right). \tag{11}$$

If equation group (9) has a solution, then the minimum value of the objective function (11) will be 0. A genetic algorithm (GA) is used to solve the above optimization problems [32], [33], [34], [35], [36]. The closer the value of the obtained objective function to 0, the more accurate the solution of the corresponding equation group (9).

According to the test data, the number of test stages is $c = 3$, and the cumulative number i_k of tests at the end of stage k, number n_k of tests, and number s_k of failures at each stage are $i_1 = 218$, $n_1 = 218$, $s_1 = 5$; $i_2 = 425$, $n_2 = 207$, $s_2 = 2$; and $i_3 = 655$, $n_3 = 230$, $s_3 = 0$. The data are substituted into objective function (11).

If the population size is 40, the probability of the variation is 0.05, and the probability of the crossover is 0.7 in the GA,

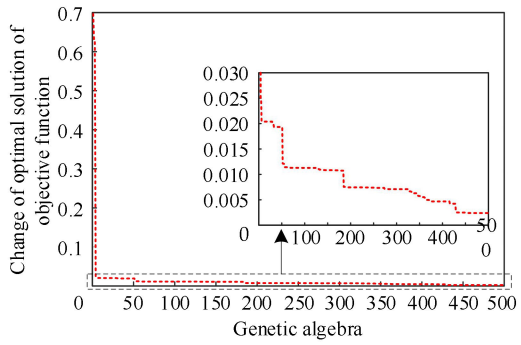

FIGURE 14. Evolution process of optimal solutions.

then the estimated values of a and b will be $\hat{a} = 0.9999$ and $\hat{b} = 0.2991$, respectively, the evolution process of the optimal solution is depicted in Figure 14. According to Figure 15, the objective function is not a multi-peak function. That is, the values of parameters $\hat{a}$ and $\hat{b}$ are the global solutions. Furthermore, according to this GA, as the number of stages k increases, i.e., as the reliability growth measures taken increase, $\hat{b}$ decreases, and the estimated value $\hat{m}$ of growth rate increases until $\hat{m} = 1 - \hat{b} = 0.7009$. According to reference [20], $\hat{m} = 0.7009$, which indicates that strong failure analysis and corrective measures have been taken.

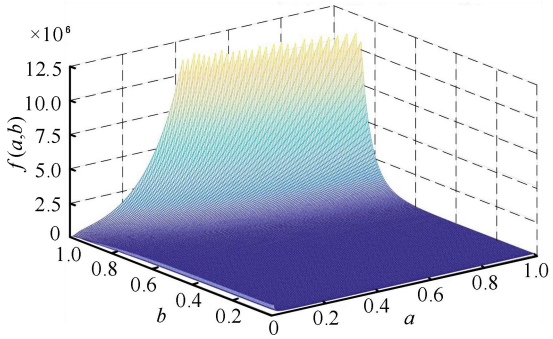

FIGURE 15. Objective function diagram.

C. TREND TEST OF RELIABILITY GROWTH

The trend test of the reliability growth is a statistical hypothesis test, which can make a probability judgment on whether the reliability of the shock absorption system of the test prototype underwent significant changes during the test. The U-test method is used to test the reliability growth trend, and the test statistic is

$$\mu = \left[\sum_{j=1}^{M} i_j' \Big/ (MJ) - \frac{1}{2} \right] \sqrt{12M} = -2.1059, \tag{12}$$

where M is the goodness-of-fit test parameter. As shown in Table 1, because the total tests of the test prototype ends in a successful manner, $M = N(655) = 7$. Let $N(i) = j$; $i_j{}'$ is the cumulative number of tests up to j failures, and J is the cumulative number of tests at the end of the testing. The selection of the significance level α involves many factors, and the smaller the value of α, the longer the required test times. However, the drawn conclusions have a high degree of confidence, taking $\alpha = 0.2$, and critical value of μ is $\mu_0 = 1.282$ by checking the table. The test statistic μ is compared with the critical value μ_0:

$$\mu < \mu_0. \tag{13}$$

Therefore, an evident reliability growth trend is observed in the shock absorption system of the test prototype when the significance level is 0.2.

D. GOODNESS-OF-FIT TEST OF AMSAA MODEL

To check whether the reliability growth data of the shock absorption system of the test prototype conform to the discrete AMSAA model, the Cramér-Von Mises test method is used to perform the goodness-of-fit test.

The goodness-of-fit test statistic $C^2(M)$ is calculated, and the equation is as follows:

$$C^2(M) = \frac{1}{12M} + \sum_{j=1}^{M} \left[\left(\frac{i_j'}{J} \right)^{\hat{b}} - \frac{2j-1}{2M} \right]^2 = 0.1112. \tag{14}$$

According to the significance level α of the test and value of the goodness-of-fit test parameter M, and after checking the table, the critical value $C^2(M, \alpha)$ of $C^2(M)$ is found to be

$$C^2(M, \alpha) = C^2(7, 0.2) = 0.1240. \tag{15}$$

The calculated value of $C^2(M)$ is compared with the critical value of $C^2(M)$, and the following equation is obtained:

$$C^2(M) < C^2(M, \alpha). \tag{16}$$

According to Equation (16), the calculated value of $C^2(M)$ is less than the critical value of $C^2(M, \alpha)$. This finding shows that the goodness-of-fit test does not reject the discrete AM-SAA model at the 0.2 significance level, and the reliability growth data conform to the AMSAA model. Thus, the discrete AMSAA model can be used to statistically estimate the reliability parameters of the shock absorption system.

E. RELIABILITY ESTIMATION AND LOWER CONFIDENCE LIMIT OF RELIABILITY

The estimated values of parameters a and b are substituted into the discrete AMSAA reliability growth model, that is, Equation (4). The reliability estimate of the final development stage (stage $k = 3$) is calculated as follows:

$$\hat{R}_k = 1 - \hat{s}_k / n_k = 1 - \hat{a} \left(i_k^{\hat{b}} - i_{k-1}^{\hat{b}} \right) \Big/ n_k = 0.9963. \tag{17}$$

According to the lower confidence limit of the reliability in the final development stage given in [37],

$$R_{k,L} = 1 - (1 - R_k) \exp \left[z_{1-\alpha} \left(2 / K_k \right)^{1/2} \right], \tag{18}$$

where $z_{1-\alpha}$ is the 1-α quantile of the standard normal distribution, and K_k is the cumulative number of failures up to stage k.

When the confidence level is $\gamma = 0.8$, the maximum likelihood estimate of the reliability lower confidence limit of the shock absorption system of the test prototype is

$$\hat{R}_{k,L} = 0.9942. \tag{19}$$

In addition, according to Equation (17) and Equation (18), based on the above GA, it can also be concluded that in the final development stage, as the number n_k of tests increases, the estimated value $\hat{R}_k$ of reliability increases, and the maximum likelihood estimate value $\hat{R}_{k,L}$ of the reliability lower confidence limit increases.

V. CONCLUSION

With regard to the problem of the mechanical claw in very few rapid secure devices (RSD) failed to capture the helicopter abdominal fixed rod due to the lose effectiveness of the internal shock absorption system of the RSD. In this study, with the delayed correction strategy, reliability analyses are conducted on the faults of the shock absorption system of a single test prototype. The causes of the faults are identified using the test+simulation research methods, and the reliability optimization designs and reliability growth tests are conducted. The following conclusions are drawn:

(1) The adoption of scheme 2 in the first test stage and scheme 1 + scheme 2 in the second test stage is correct and feasible for the reliability optimization design of the shock absorption system, and the robustness of the system is improved. According to the reliability growth test data, the number of test failures in each stage is gradually reduced until all the tests in the third stage are successful. the U-test method also shows that the shock absorption system of the test prototype has obvious reliability growth trend, and the confidence level is 80%.

(2) Reliability growth tests after the optimized design of the shock absorption system of the test prototype can be statistically and inferentially performed using a discrete AM-SAA reliability growth model. The statistical and inference results show that in the third test stage, the reliability point estimation of the test prototype is 99.63%, and the confidence lower limit of the reliability interval estimation with a confidence degree of 80% is 99.42%. Meanwhile, based on the success of all tests on the test prototype in the third test phase, it can be explained that the reliability growth measures taken are effective and meet the requirement that the RSD reliability is not less than 99.50% to a certain extent. This study further provides data support for the reliability research of RSD, which is of great significance in improving the reliability and serviceability of RSD equipment and ensuring the rate of attendance and life safety of shipboard helicopter under severe sea conditions.

ACKNOWLEDGMENT

Author Contributions: Zhuxin Zhang: Designed the system structure, analyzed the working principle of the system, designed the reliability growth test bench, and analyzed the cause of the failure; Weijian Li: Analyzed the cause of the failure, performed the reliability growth test, conducted statistical estimation of test data using the discrete ASMAA model, and wrote the article; Huiliang Sun: Helped to calculate the model parameters using the GA; Bing Wang: Contributed to the experiments. Dingxuan Zhao: Provided financial support for this study; Tao Ni: Checked the relevant calculation for the model and interpretation of the conclusion, and contributed to the research background.

REFERENCES

[1] W. Feng and C. Lv, "Impact of shipborne helicopter technology development on mission capability," *Helicopter Technique*, vol. 49, no. 2, pp. 64–67, Jun. 2020.
[2] B. Li, X. Wang, X. Xu, and C. Yang, "Study on assisted landing technology for shipboard helicopter based on computer vision," *Acta Armamentarii*, vol. 28, no. 3, pp. 370–373, Mar. 2007.
[3] B. Wang, P. Jiang, H. Zhang, and C. Wang, "Risk and counter-measure of taking off and landing on ship in high sea condition," *Ship Eng.*, vol. 43, no. S2, pp. 9–13, Nov. 2021.
[4] W. Tan and Y. Cao, "Simulation of flow field and calculation of safe operating envelope of shipborne helicopter based on chimera grid," *J. Aerosp. Power*, vol. 35, no. 10, pp. 2166–2175, Oct. 2020.
[5] Z. Zhang, W. Li, D. Zhao, B. Wang, T. Ni, and T. Jia, "Research on reliability growth of chain transmission system in rapid secure device of shipborne helicopter," *IEEE Access*, vol. 11, pp. 3198–3207, 2023.
[6] B. Sun, "Assisted landing device for shipboard helicopter," *Modern Weaponry*, vol. 18, no. 10, pp. 37–38, Oct. 1995.
[7] X. Liang, "Analysis on dynamic characteristics of shipborne helicopter assisted deck-landing," M.S. thesis, Dept. Aerosp. Eng., Nanjing Univ. Aeronaut. Astronaut., Nanjing, China, 2018.
[8] Z. Yu, "Development of shipboard helicopter pulling and lowering device," *Helicopter Technique*, vol. 27, no. 4, pp. 40–43, Nov. 1998.
[9] W. G. Stewart and A. Baekken, "Helicopter rapid securing device," US Patent 3 303 807, Feb. 14, 1967.
[10] B. Fu, "Take-off and landing and landing aid of a shipboard helicopter," *Flight Test*, vol. 14, no. 2, pp. 65–81, 1990.
[11] N. Ju, "A new type of helicopter landing assistant device-ASIST system," *Ship Demonstration Reference*, vol. 5, no. 1, pp. 32–38, 1996.
[12] H. Wu, D. Tan, Q. Li, S. He, and X. Zhang, "Comparative analysis on the comprehensive performance of foreign shipborne helicopter assist secure and traverse equipment," *Ship Sci. Technol.*, vol. 43, no. 23, pp. 185–189, Dec. 2021.
[13] Y. Xu, "The strategy of shipboard helicopter safe path planning," M.S. thesis, Dept. Aerosp. Eng., Nanjing Univ. Aeronaut. Astronaut., Nanjing, China, 2020.
[14] T. Wei and Y. Tian, "Development and application of Chinese Navy's Zhi-9 shipborne helicopter," *Shipborne Weapons*, vol. 16, no. 5, pp. 48–61, May 2008.
[15] H. Wu, D. Tan, Q. Li, and S. He, "Development trend analysis of a technical system of foreign helicopter assist secure and traverse Equipment," *Ship Eng.*, vol. 43, no. S2, pp. 49–52, Nov. 2021.
[16] X. Chang, "Landing aid device of a shipborne helicopter," *Ordnance Knowl.*, vol. 35, no. 10, pp. 78–81, Oct. 2013.
[17] J. Zhang, "Design and control of an air-surface cooperation oriented auto take-off and land system," M.S. thesis, Dept. Mechatronic Eng., Shenyang Ligong Univ., Shenyang, China, 2017.
[18] D. Zhao, Z. Zhang, Z. Sun, and X. Ai, "A hydraulic system and control method for a helicopter rapid secure device operating at sea," C Patent 1 146 881 14B, Jan. 3, 2023.
[19] H. Zhang, B. Cai, C. Zhang, T. Xu, H. Zhao, Z. Zhang, D. Zhu, Y. Zhang, and F. Liu, "A safe and quick recovery and release system and method for the helicopter operating at sea," C Patent 1 093 987 35B, Jul. 31, 2020.
[20] W. Mei, *Reliability Growth Test*, 1st ed. Beijing, China: National Defense Industry Press, 2002, pp. 16–53.

[21] J. Zhang, C. Li, and X. Feng, "Research on reliability growth model of success or failure products," *Qual. Rel.*, vol. 17, no. 6, pp. 19–31, Dec. 2002.
[22] J. T. Duane, "Learning curve approach to reliability monitoring," *IEEE Trans. Aerosp.*, vol. AS-2, no. 2, pp. 563–566, Apr. 1964.
[23] L. H. Crow, "Confidence interval procedures for the Weibull process with applications to reliability growth," *Technometrics*, vol. 24, no. 1, pp. 67–72, Feb. 1982.
[24] L. H. Crow and A. P. Basu, "Reliability growth estimation with missing data. II," in *Proc. Annu. Rel. Maintainability Symp.*, Los Angeles, CA, USA, Jan. 1988, pp. 476–483.
[25] A. Fries and A. Sen, "A survey of discrete reliability-growth models," *IEEE Trans. Rel.*, vol. 45, no. 4, pp. 582–604, Dec. 1996.
[26] Z. Jingyi, Z. Ming, W. Qiming, C. Wei, R. Qiang, L. Wenlei, and S. Shaopeng, "Reliability growth test study of five-hundred-meter aperture spherical radio telescope reflective surface hydraulic actuator," *J. Mech. Eng.*, vol. 55, no. 16, p. 197, 2019.
[27] L. Zhou, "Research on parameters solution of discrete AMSAA reliability growing model based on EP algorithm," M.S. thesis, Dept. Precision Instrum. Machinery, Harbin Univ. Sci. Technol., Harbin, China, 2013.
[28] F. Liu and W. Zhang, "Analysis on reliability growth of solid rocket motor based on AMSAA discrete model," *J. Solid Rocket Technol.*, vol. 29, no. 1, pp. 22–24, Feb. 2006.
[29] F. Liu, "Research on methods and applications of reliability growth test for solid rocket motor," Ph.D. thesis, Dept. Aeronaut. Astronaut. Sci. Technol., National Univ. Defense Technol., Changsha, China, 2006.
[30] H. Lv, X. Dai, P. Wang, and Y. Yu, "Application of AMSAA discrete model in analysis and assessment of rocket motor reliability growth," *J. Projectiles, Rockets, Missiles Guid.*, vol. 28, no. 1, pp. 171–176, Feb. 2008.
[31] A. Fries, "Discrete reliability-growth models based on a learning-curve property," *IEEE Trans. Rel.*, vol. 42, no. 2, pp. 303–306, Jun. 1993.
[32] L. Yu, F. Shi, H. Wang, and F. Hu, *Analysis of 30 Cases of MATLAB Intelligent Algorithm*, 2st ed. Beijing, China: Beijing University of Aeronautics and Astronautics Press, 2015, pp. 1–16.
[33] C. Lu, D. Fang, W. Chen, and W. Qian, "MLEs of beta distribution parameters based on genetic algorithm," *J. Jishou Univ.*, vol. 37, no. 5, pp. 13–15, Sep. 2016.
[34] J. Qu, "A study of system reliability optimization using genetic algorithm," M.S. thesis, Dept. Mech. Manuf. Automat., Dalian Univ. Technol., Dalian, China, 2006.
[35] Z. Mao, B. Song, Z. Li, and H. Hu, "Optimization method of maximum likelihood estimation parameter estimation based on genetic algorithms," *J. Mech. Strength*, vol. 28, no. 1, pp. 79–82, Feb. 2006.
[36] T. Zhang, C. Teng, and Z. Han, "Application of genetic algorithms to system reliability optimization," *Control Decis.*, vol. 17, no. 3, pp. 378–380 and 384, May 2002.
[37] R. A. Johnson, "Confidence estimation with discrete reliability growth models," *J. Stat. Planning Inference*, vol. 29, nos. 1–2, pp. 87–97, Sep. 1991.

ZHUXIN ZHANG received the B.E. degree in fluid power transmission and control from the Northeastern University of Technology, Shenyang, China, in 1986, the M.E. degree in fluid power transmission and control from the Northeastern University, Shenyang, in 1996, and the Ph.D. degree in mechanical and electronic engineering from Jilin University, Changchun, China, in 2009. He is currently a Professor and the Ph.D. Supervisor with the Hebei Key Laboratory of Special Delivery Equipment, Yanshan University. He has conducted several projects with the National Key Technology Research and Development Program and the Key Research and Development Program of Province. His current research interests include equipment reliability, engineering robot technology, electrohydraulic control technology, and research on mechanism and robot technology.

WEIJIAN LI received the B.E. degree in fluid power transmission and control from the School of Liren, Yanshan University, Qinhuangdao, China, in 2015, and the M.E. degree in fluid power transmission and control from Yanshan University in 2018, where he is currently pursuing the Ph.D. degree with the Hebei Key Laboratory of Special Delivery Equipment. His current research interests include reliability research of equipment and fluid power transmission and control.

HUILIANG SUN received the B.E. degree in mechanical design, manufacture and automation from the Hefei University of Technology, Hefei, China, in 2013. He is currently pursuing the M.E. degree with the Hebei Key Laboratory of Special Delivery Equipment, Yanshan University. His current research interests include advanced design technology and electro-hydraulic servo control.

BING WANG received the B.E. degree from the Henan Institute of Engineering, Zhengzhou, China, in 2017. He is currently pursuing the M.E. degree with the Hebei Key Laboratory of Special Delivery Equipment, Yanshan University. His current research interests include advanced design technology and reliability research of equipment.

DINGXUAN ZHAO received the B.E. degree in mechanical engineering from the Xi'an University of Architecture and Technology, Xi'an, China, in 1985, and the M.E. and Ph.D. degrees in engineering machinery from the Jilin University of Technology, Changchun, China, in 1988 and 1992, respectively. He is currently a Professor and the Ph.D. Supervisor with the Hebei Key Laboratory of Special Delivery Equipment, Yanshan University, where he is also the President. He has conducted several projects with the National Key Technology Research and Development Program and the Key Research and Development Program of Province. His current research interests include dynamics and simulation of complex mechanical systems, automatic transmission and energy saving control of construction vehicles, pavement spectrum acquisition and reproduction technology, and engineering robot technology.

TAO NI received the B.E. degree in mechanical and electronic engineering from Shandong University Technology, Zibo, China, in 2000, and the M.E. and Ph.D. degrees in mechanical and electronic engineering from Jilin University, Changchun, China, in 2003 and 2006, respectively. He is currently a Professor and the Ph.D. Supervisor with the School of Vehicle and Energy, Yanshan University. His current research interests include intelligent mobile robot technology, virtual reality, and simulation technology.